



# “Nano-on-Micro” approach enables synthesis of ZnO nano-cactus for gas sensing applications



Monsur Islam<sup>a,\*</sup>, Alok K. Srivastava<sup>b</sup>, Basavanakote M. Basavaraja<sup>c</sup>, Ashutosh Sharma<sup>d</sup>

<sup>a</sup> Institute of Microstructure Technology, Karlsruhe Institute of Technology, Hermann-von-Helmholtz-Platz 1, 76344, Eggenstein-Leopoldshafen, Germany

<sup>b</sup> Defence Materials and Stores R.D Establishment (DRDO), GT Road, Kanpur, 208013, India

<sup>c</sup> Department of Science Humanities, PES University, Bengaluru, Karnataka, 560085, India

<sup>d</sup> Department of Chemical Engineering, Indian Institute of Technology, Kanpur, 208016, Uttar Pradesh, India

## ARTICLE INFO

### Keywords:

Electrospinning  
Zinc oxide nanostructure  
Vapor-liquid-solid  
Gas sensor

## ABSTRACT

We report a “nano-on-micro” approach for growth of a cactus-like nanostructures of zinc oxide (ZnO) for gas sensing application. We use electrospun polymeric fibers doped with catalyst nanoparticles as the template and employ a vapor-liquid-solid (VLS) method to growth of the ZnO nanostructures. Controlling the processing variables in the VLS process yields to growth of needle-like nanostructures of ZnO around the electrospun fibers, which resembles the needles of a cactus. The ZnO nano-cactus features wurtzite ZnO like crystal structure. We investigate the gas sensing capabilities of the ZnO nano-cactus. The ZnO nanostructures show high sensitivity and selectivity for sensing of ethanol gas. The “nano-on-micro” approach enables single step deposition of nano-materials between electrodes during synthesis, which eliminates post-synthesis steps, and thus demonstrates better compatibility towards device integration for metal oxide nanostructures.

## 1. Introduction

Nanostructures of metal oxides have been extensively investigated for sensing applications for more than five decades, due to their high surface-to-volume ratio, and excellent semiconducting properties [1–3]. Several semiconductor metal oxides (SMOs) have been explored, which includes tin oxide (SnO<sub>2</sub>) [4,5], zinc oxide (ZnO) [6,7], titanium oxide (TiO<sub>2</sub>) [8, 9], and indium oxide (In<sub>2</sub>O<sub>3</sub>) [10,11]. These metal oxides have been mostly studied in form of thin and thick films. In 1991, Yamazoe reported that dimensional reduction of the metal oxide semiconductors improved the sensing performance of the metal oxides [12]. Since then, significant efforts have been made to reduce the dimensions of SMOs to several nanometers, which resulted in synthesis of a variety of one dimensional nanostructures [13–15].

Among several semiconductor metal oxides, ZnO has been extensively studied due to its low toxicity, high thermal stability, good oxygen resistivity, good biocompatibility and high electron mobility [16–18]. Furthermore, ZnO exhibits wide direct band gap ( $E_g = 3.37$  eV) and large

exciton binding energy (60 meV). These properties have enabled ZnO as a preferable candidate for solid state sensors. The sensing capabilities of solid state sensor materials are strongly related to the composition, morphology, and crystalline size of the sensing material. In order to enhance the sensitivity of ZnO based solid state sensors, a number of nanostructures of ZnO has been synthesized and investigated for sensing performances, which includes nanowire, nanofiber, nano-needle, nanocomb, and nanobelt [6,19–22]. Although these nanostructures have delivered exciting results, there still needs more research in search for novel nanostructures of ZnO, which can result in even higher sensitivity and higher selectivity. Furthermore, integration of the nanostructures to a sensor device remains a challenge, as it typically needs post-synthesis processes, such as mixing of the nanostructures with polymers in slurry form [23,24]. Therefore, there is still a requirement for simpler device integration for metal oxide nanostructures, which can be applied for real world applications.

Towards obtaining a nanostructure with a high surface area and easier device integration, we postulate a “nano-on-micro” approach,

\* Corresponding author.

E-mail addresses: [monsur.islam@kit.edu](mailto:monsur.islam@kit.edu), [monsurislam79@gmail.com](mailto:monsurislam79@gmail.com) (M. Islam).



Production and hosting by Elsevier

<https://doi.org/10.1016/j.sintl.2021.100084>

Received 21 December 2020; Received in revised form 22 January 2021; Accepted 23 January 2021

Available online 5 February 2021

2666-3511/© 2021 The Authors. Production and hosting by Elsevier B.V. on behalf of KeAi Communications Co., Ltd. This is an open access article under the CC BY-

NC-ND license (<http://creativecommons.org/licenses/by-nc-nd/4.0/>).

where the metal oxide nanostructures can be grown on a micron-scale template. We choose electrospun nanofibers as the micron-scale template due to their intrinsic high surface-to-volume ratio and ease of fabrication [25,26]. Several researchers have reported growth of ZnO nanowires around electrospun nanofibers using hydrothermal and electrodeposition routes of metal oxide growth [27–31]. However, these methods include an intermediate step of seeding the electrospun fibers with ZnO or Zn nanoparticles, which facilitates the growth of ZnO nanowires in the subsequent nanowire growth step. The seeding process is non-selective, which yields growth of metal oxides invasively. Hence, the device results in undesired interference from the excess metal oxide growths. Such phenomenon restricts the use of such methodology from direct integration of the ZnO nanostructures with a working device.

Here, we use vapor-liquid-solid (VLS) method for growth of ZnO nanostructures around electrospun polymer fibers in the “nano-on-micro” approach. To the best of our knowledge, this is the first report on integration of electrospinning and VLS method for metal oxide nanostructure growth. To facilitate the ZnO growth in VLS method, we use a polyacrylonitrile (PAN)/gold nanoparticle (AuNP) composite for electrospinning, where AuNPs serve as the catalyst for ZnO growth. Using such catalyst-embedded fibers can enable the selective growth of the ZnO nanowires only around the electrospun fibers, which can yield to fabrication a clean device resulting in less interference due to undesired growth of metal oxides. We optimize the processing variables of the VLS method to grow long needle-like ZnO nanowires around the electrospun fibers, which resemble to needles of a cactus. We further demonstrate the gas sensing capabilities of the novel ZnO nano-cactus

structures, which may be attributed to the “nano-on-micro” approach adopted for synthesis of the novel ZnO nanostructures.

## 2. Materials and methods

### 2.1. Materials

The chemicals polyacrylonitrile (PAN) and N,N-Dimethylformamide (DMF) were purchased from Sigma Aldrich, India and used as received. Gold nanoparticles (AuNPs) having diameter of  $4.9 \pm 0.6$  nm dissolved in 0.002 M toluene were used as the catalysts for the synthesis of ZnO nanostructures. Quartz was used as the substrate because it can sustain high temperature required for the ZnO synthesis. A square quartz substrate ( $2 \text{ cm} \times 2 \text{ cm}$ ) was patterned with lines or interdigitated electrodes with inter electrode distance in the range 20–100  $\mu\text{m}$ .

### 2.2. Experimental process

The fabrication process is schematically presented in Fig. 1. To prepare the solution for electrospinning, the AuNPs were first dispersed in DMF through ultra sonication for 30 min 8% (wt.%) PAN was added to the AuNPs/DMF solution and put it on a magnetic stirrer at  $65^\circ\text{C}$  for 8 h to yield a homogeneous solution for electrospinning. Electrospinning of the PAN/AuNP composite solution was performed using an electric field of 2 kV/cm and flow rate of 1 ml/h. The quartz substrate was clamped with the rotating drum collector so that the electrospun fibers could be collected across the patterned silver lines on the quartz.

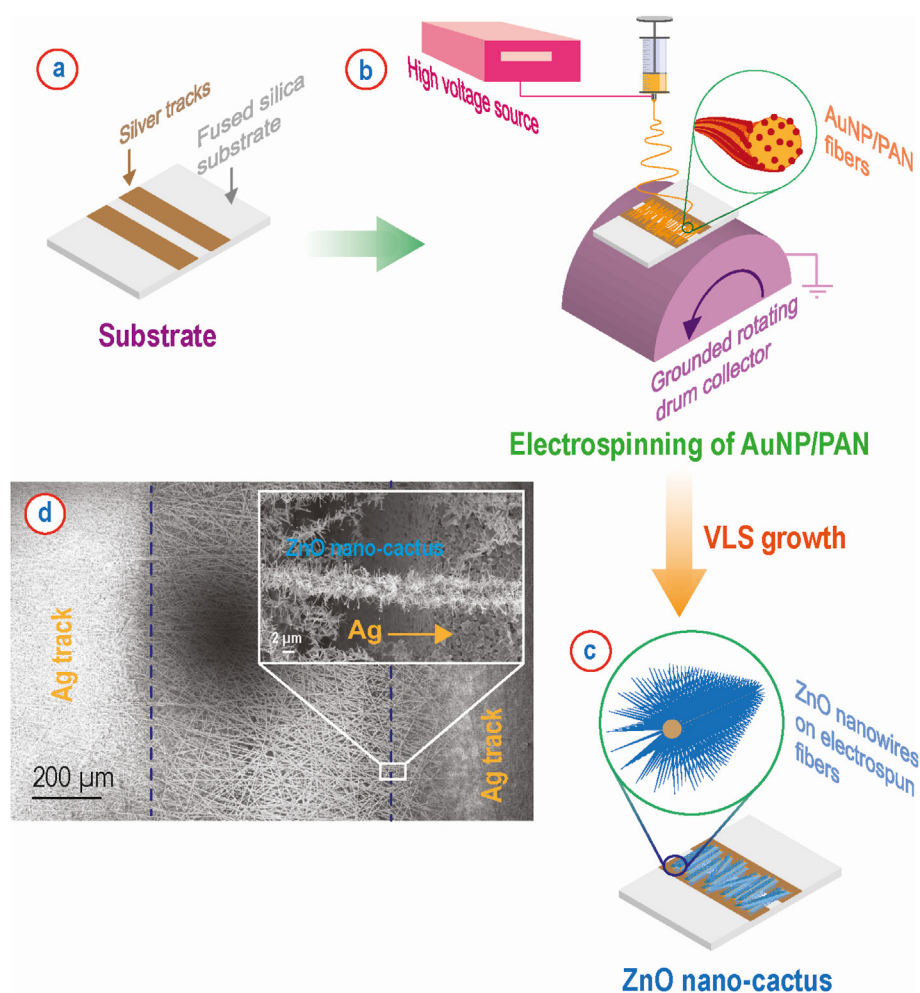


**Fig. 1.** Schematic representation of the experimental procedure for growth of ZnO nano-cactus. The process includes (a) patterning of silver electrodes on a fused silica substrate, (b) electrospinning of AuNP/PAN fibers across the silver tracks, and (c) VLS growth of ZnO nanowires around electrospun fibers, which resemble to cactus-like features. (d) SEM image showing the alignment of the ZnO nanostructures on the fibril structures across the silver tracks. The inset shows a suspended structure on the edge of the silver track.

The electrospun PAN/AuNP composite fibers were subjected to vapor-liquid-solid (VLS) method for growth of ZnO nanostructures. To prepare the precursor material, ZnO powder was mixed with graphite powder in a weight ratio of 1:1. 10 g of such powder mixture was taken in an alumina crucible and placed in the reaction zone (RZ) of a three-zone furnace. The electrospun PAN/AuNPs fibers on the quartz substrate was placed in the deposition zone (DZ) of the furnace, which is 10 cm downstream from the RZ. For VLS growth of ZnO, the parameters of interest in our experiments were temperature of the RZ ( $T_{RZ}$ ), temperature of the DZ ( $T_{DZ}$ ) and reaction time. We varied the  $T_{RZ}$  from 900 °C to 1100 °C, whereas the  $T_{DZ}$  was varied from 400 °C to 550 °C. The reaction time was varied from 30 min to 45 min. A constant flow of argon gas was maintained at 150 standard cubic centimeters per minute (sccm) throughout the entire process.

### 2.3. Material characterization

The samples obtained in the deposition zone were characterized by X-ray diffraction (XRD, Xâ€™Pert Pro, PAN Analytical, Netherlands) equipped with graphite monochromatized high intensity Cu K $\alpha$ ±1 radiation ( $\lambda = 1.5405 \text{ \AA}$ ) to characterize the composition and crystallinity of the deposited material. Raman scattering at room temperature was performed using WiTec, Germany, using a laser beam with wavelength of 532 nm to study the vibrational properties of ZnO nanowires. Microstructures of the nanoforms were investigated by field emission scanning electron microscope (FESEM, Supra 400VP, Zeiss, USA) and transmission electron microscope (TEM, Tecnai G2, USA).

### 2.4. Gas sensing

Gas sensing properties of the ZnO nanostructures on the quartz substrate were investigated by measuring the change of current upon exposure to for 10–500 ppm ethanol (CH<sub>3</sub>CH<sub>2</sub>OH) and acetone (CH<sub>3</sub>COCH<sub>3</sub>) gas at 230 °C. ZnO nanostructure sensor was placed in a homemade closed chamber and platinum electrodes were fixed with the silver tracks patterned on the quartz substrate with the help of silver paste. Then the system was heated at 300 °C for 15 min to ensure string connect between platinum electrodes and silver tracks. An air flow at 600 ml/min was maintained to the chamber to stabilize the system before sensor testing at the elevated temperature. For gas sensing, desired amount of target gas was injected into the system and the change of the current was measured as a function of time at a constant voltage of 0.2 V using a Keithley 6517 picoammeter. When the value of current reached to a steady state, the chamber was purged with air until a constant value of current was obtained. Next set of data was recorded when a constant value of current at the baseline was obtained. The sensitivity of the ZnO nanostructures was calculated using Equation (1), which is ratio of steady

state current ( $I_g$ ) achieved when ZnO nanostructures were exposed to the target gas to the steady state current in air ( $I_a$ ).

$$\text{Sensitivity} = \frac{I_g}{I_a} \quad (1)$$

## 3. Results and discussions

### 3.1. Material characterization of grown nanostructures

A white wool-like material was obtained on the substrate in the deposition zone of the furnace after the VLS process. The composition of the white material was confirmed using x-ray diffraction (XRD). The XRD pattern is presented in Fig. 2a. Major peaks of the XRD pattern were indexed to typical wurtzite ZnO [32,33] and matched with Pearson's Crystal Data (PCD) card number 1218650. This confirms that the material deposited on the substrate in the deposition zone was ZnO. The sharp feature of the ZnO peaks indicates good crystallinity of the ZnO. The phases of the ZnO crystal planes are indexed in the XRD diffractogram in Fig. 2a. In addition to the peaks of the ZnO, several other peaks were also observed at  $2\theta = 38.08^\circ$ ,  $44.26^\circ$ ,  $64.36^\circ$ , and  $77.32^\circ$ . These peaks are attributed to the Ag and Au [34,35], as Au and Ag exhibit almost similar XRD pattern [36]. The Ag appeared in the XRD pattern because of the Ag tracks patterned on the substrate. The presence of Au was attributed to the Au nanoparticles used as the catalyst for the ZnO growth. Furthermore, a peak at  $2\theta = 30.6^\circ$  was also observed in the XRD pattern, which can be indexed to the quartz substrate [37]. A bulge section was also observed in the XRD diffractogram in between  $2\theta = 20^\circ$  to  $2\theta = 26^\circ$ , which can be indexed to (002) reflection of turbostratic carbon [38,39]. This was attributed to the carbonization of the electrospun PAN fibers at high temperature. The minimum temperature used in the deposition zone was 400 °C. At such temperature, the PAN fibers must have already turned into a carbon rich material [40].

Raman spectra (Fig. 2b) of the synthesized material further confirms the growth of ZnO. According to Group Theory, ZnO can exhibit eight sets of optical modes, among which A<sub>1</sub>, E<sub>1</sub> and E<sub>2</sub> are Raman active for ZnO single crystal structures [41,42]. A<sub>1</sub> and E<sub>1</sub> are polar modes, and active to Raman and infrared, whereas E<sub>2</sub> is non-polar modes and only active to Raman [43]. The peaks in the Raman spectra obtained for the grown material are labeled and assigned to their corresponding phonon modes [42]. The dominant peak for ZnO was indexed at  $439 \text{ cm}^{-1}$ , which corresponds to E<sub>2H</sub> mode representing the intrinsic characteristics of Raman active mode of wurtzite hexagonal ZnO [41–43]. The peak at  $570 \text{ cm}^{-1}$  was attributed to the A<sub>1L</sub> mode of ZnO. The E<sub>2L</sub> modes of ZnO are indexed at  $\sim 99 \text{ cm}^{-1}$  and  $\sim 200 \text{ cm}^{-1}$ . A peak for Si substrate can be also observed at  $525 \text{ cm}^{-1}$  [44]. It should be noted here that, unlike the XRD diffractogram, no distinct peaks for carbon were observed in the

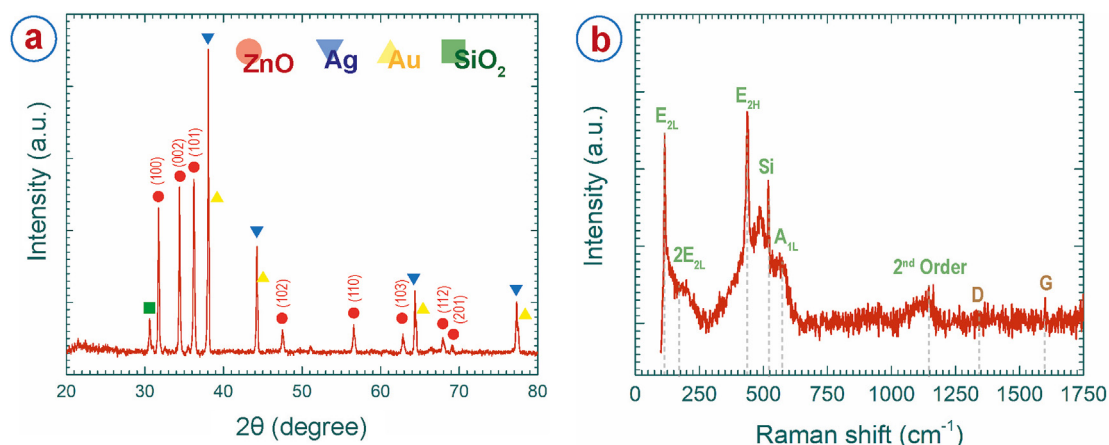


Fig. 2. (a) XRD pattern and (b) Raman spectra of the ZnO synthesized around the electrospun fibers.

Raman spectra. We indicated the position of characteristic D and G-band of carbon in the Raman spectra at  $1350\text{ cm}^{-1}$  and  $1585\text{ cm}^{-1}$ , respectively. The relative intensity of the Raman peaks of ZnO was significantly stronger than the carbon peaks. Therefore, the carbon peaks might have coincided within the noise of the Raman intensity.

### 3.2. Growth of ZnO nano-cactus on electrospun fibers

As mentioned earlier, ZnO nanostructures were grown on the electrospun PAN/AuNP fiber template. Field emission scanning electron microscopy (FESEM) image of the electrospun fibers is shown in Fig. 3a; these fibers featured an average diameter of  $709 \pm 62.08\text{ nm}$ . The growth of the ZnO nanostructure was controlled by varying  $T_{RZ}$ ,  $T_{DZ}$  and reaction time. We started the experiments using a  $T_{RZ}$  of  $900\text{ }^\circ\text{C}$  and  $T_{DZ}$  of  $400\text{ }^\circ\text{C}$  and reaction duration of 45 min. Such conditions resulted in growth of non-uniformly distributed large crystallites of ZnO on the carbonized fibril structures (Fig. 3b). Increase of the  $T_{RZ}$  to  $1100\text{ }^\circ\text{C}$  did not show any improvement in the ZnO morphology (Fig. 3c). However, the crystallite size seemed bigger than that for  $T_{RZ}$  of  $900\text{ }^\circ\text{C}$ . Increasing the  $T_{DZ}$  to  $500\text{ }^\circ\text{C}$  keeping  $T_{RZ}$  constant at  $1100\text{ }^\circ\text{C}$  yielded a uniform and large bead-like morphology around the fibrils as shown in Fig. 3d. With further increase of  $T_{DZ}$  to  $550\text{ }^\circ\text{C}$ , a uniform nanowire like morphology can be observed around the fibers (Fig. 3e). Higher magnification SEM shows that these nanowires feature bead-like nanostructures (inset of Fig. 3e). Keeping the  $T_{DZ}$  constant at  $550\text{ }^\circ\text{C}$ , we decreased the  $T_{RZ}$  to  $1000\text{ }^\circ\text{C}$ . This resulted in growth of a uniform, long and fat leaves like ZnO nanostructure (Fig. 3f). At the same  $T_{RZ}$  and  $T_{DZ}$ , we shortened the reaction time from 45 min to 30 min, which resulted in a more long needle-like nanostructure (Fig. 3g and h). However, these needle-like morphology resembles the needles of a cactus as shown in Fig. 3h. This sample is further referred as ZnO nano-cactus. At the tip of these nano-cactus, the catalyst alloy droplet can be also observed, as indicated by the dotted red

circles in Fig. 3i. This confirms a bottom-up catalyst-assisted growth of the ZnO nanostructures. The inset of Fig. 3i shows the energy-dispersive X-ray (EDX) spectra of the ZnO nano-cactus structures, showing the presence of elemental Zn and oxygen, which further confirms the formation of ZnO complementing XRD and Raman spectra. Elemental Si can be also observed in the EDX spectra, which is attributed to the quartz substrate.

The ZnO nano-cactus was further investigated using transmission electron microscopy (TEM) images as shown in Fig. 4a, which presents the TEM image of a single nanowire of the ZnO nano-cactus. It was evident that the ZnO featured needle-like structure with reducing diameter from base to its tip. The diameter of the base was around  $200\text{ nm}$ , whereas the diameter of the tip was around  $20\text{ nm}$ . The length of the nanowires was in the range  $3\text{ }\mu\text{m}$  to  $5\text{ }\mu\text{m}$ . The crystal arrangement in the nanoform can be seen in the Fig. 4b. The high magnification TEM image showed the crystal planes with d-spacing of  $0.26\text{ nm}$  and  $0.28\text{ nm}$ , which can be attributed to the (002) and (100) planes of ZnO, respectively. This also confirms the wurtzite crystal structure of the VLS-grown ZnO [45–47].

The electron microscopy images showed that morphology of the ZnO nanostructures has a strong dependence on the  $T_{RZ}$ ,  $T_{DZ}$  and reaction time. All these three parameters appeared to have proportional relation on the shape and size of the ZnO nanostructures. In other words, increasing of these parameters resulted in larger nanostructures. This is in agreement with the previous reports of nanostructure growth in VLS method [48–51]. For ZnO nanostructure growth in VLS method, the process starts with reduction of ZnO to Zn vapor in presence of graphite particles at a high temperature [52,53], which is further transported to relatively lower temperature deposition zone by an inert gas. The reduction rate of ZnO increases with the increase of  $T_{RZ}$ . Hence, increasing  $T_{RZ}$  supplies higher amount of Zn vapor to the deposition zone [54]. In the deposition zone, the Zn vapor and the Au nanoparticles form

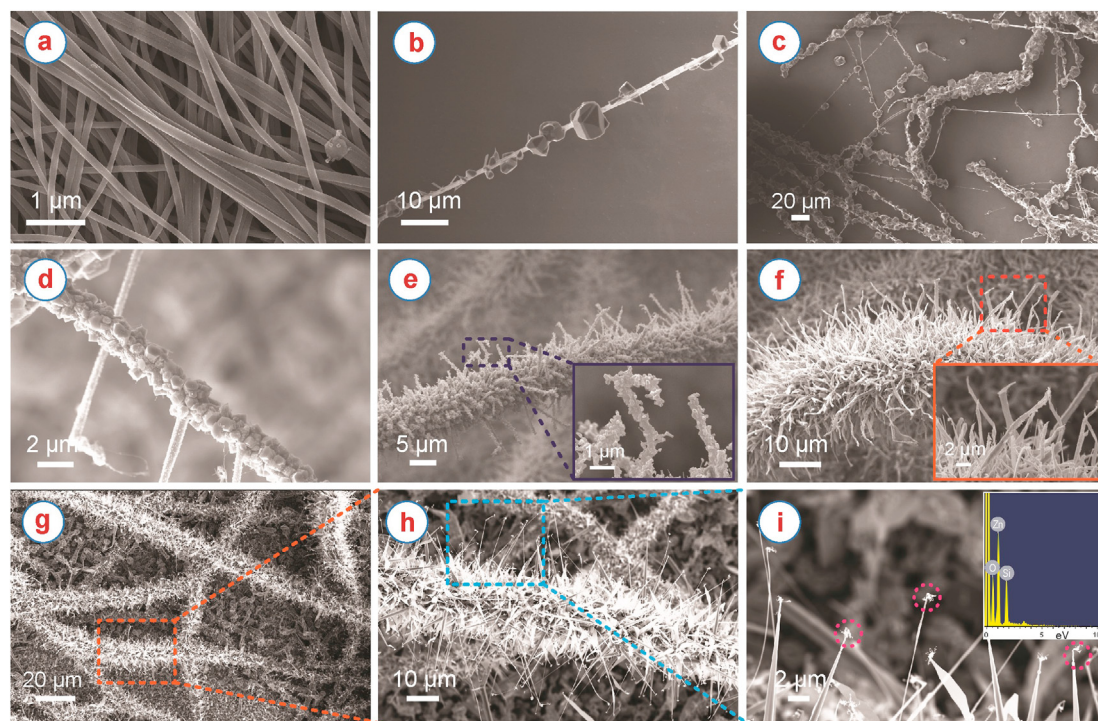


**Fig. 3.** (a) SEM of electrospun PAN-AuNPs nanofibers. SEM of the ZnO nanostructures grown on the electrospun fibers at different conditions: (b)  $T_{RZ} = 900\text{ }^\circ\text{C}$ ,  $T_{DZ} = 400\text{ }^\circ\text{C}$ , reaction time = 45 min; (c)  $T_{RZ} = 1100\text{ }^\circ\text{C}$ ,  $T_{DZ} = 400\text{ }^\circ\text{C}$ , reaction time = 45 min; (d)  $T_{RZ} = 1100\text{ }^\circ\text{C}$ ,  $T_{DZ} = 500\text{ }^\circ\text{C}$ , reaction time = 45 min; (e)  $T_{RZ} = 1100\text{ }^\circ\text{C}$ ,  $T_{DZ} = 550\text{ }^\circ\text{C}$ , reaction time = 45 min; (f)  $T_{RZ} = 1000\text{ }^\circ\text{C}$ ,  $T_{DZ} = 550\text{ }^\circ\text{C}$ , reaction time = 45 min; (g)  $T_{RZ} = 1100\text{ }^\circ\text{C}$ ,  $T_{DZ} = 550\text{ }^\circ\text{C}$ , reaction time = 30 min. Inset of (e) and (f) shows higher magnification SEM images of their corresponding nanostructures. (h) Higher magnification SEM image of the dashed section drawn in (g), showing ZnO nano-cactus around the electrospun fibers. (i) Higher magnification SEM image of the dashed section of (h), showing nano-cactus like features and presence of Au nanoparticle at the tip of the nanostructures as indicated by the dotted red circles. Inset of (i) shows EDX spectra of the ZnO nano-cactus structures.

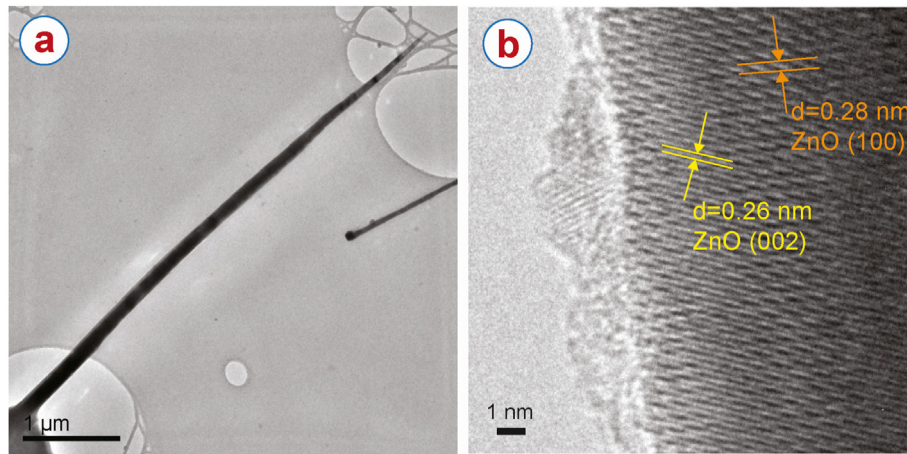


Fig. 4. (a) TEM image of single ZnO nanostructure, showing cactus thorn-like feature. (b) Higher magnification TEM image of ZnO nanostructure, showing crystal planes with d-spacing of 0.26 nm and 0.28 nm, which are attributed to the (002) and (100) planes of ZnO, respectively.

an eutectic liquid alloy. Once the Zn saturates in the alloy droplet, and reacts with ambient oxygen, ZnO nuclei start crystallizing on the substrate. In this work, the nucleation of the ZnO structures exhibited strong dependence on  $T_{DZ}$ , as incomplete and irregular deposition was observed at  $T_{DZ}$  of 400 °C, irrespective of  $T_{RZ}$  and reaction time. This might be due to non-availability of the minimum activation energy required for the VLS growth, which led to crystal growth in all directions. Furthermore, higher  $T_{RZ}$ , as inferred from the VLS mechanism, resulted in higher Zn vapor concentration in the deposition zone, which yielded formation of larger particles. Similarly, longer reaction time yielded a larger ZnO

structures. Therefore, to grow the ZnO nano-cactus structures, the Zn vapor supply to the deposition zone needed to be controlled by regulating  $T_{RZ}$  and reaction time, whereas deposition of ZnO was controlled by regulating  $T_{DZ}$ .

### 3.3. Gas sensing properties

The ZnO nano-cactus structures were tested for gas sensing using ethanol and acetone. The gas sensing performance was investigated for a gas concentration ranging from 10 ppm to 500 ppm and at a temperature

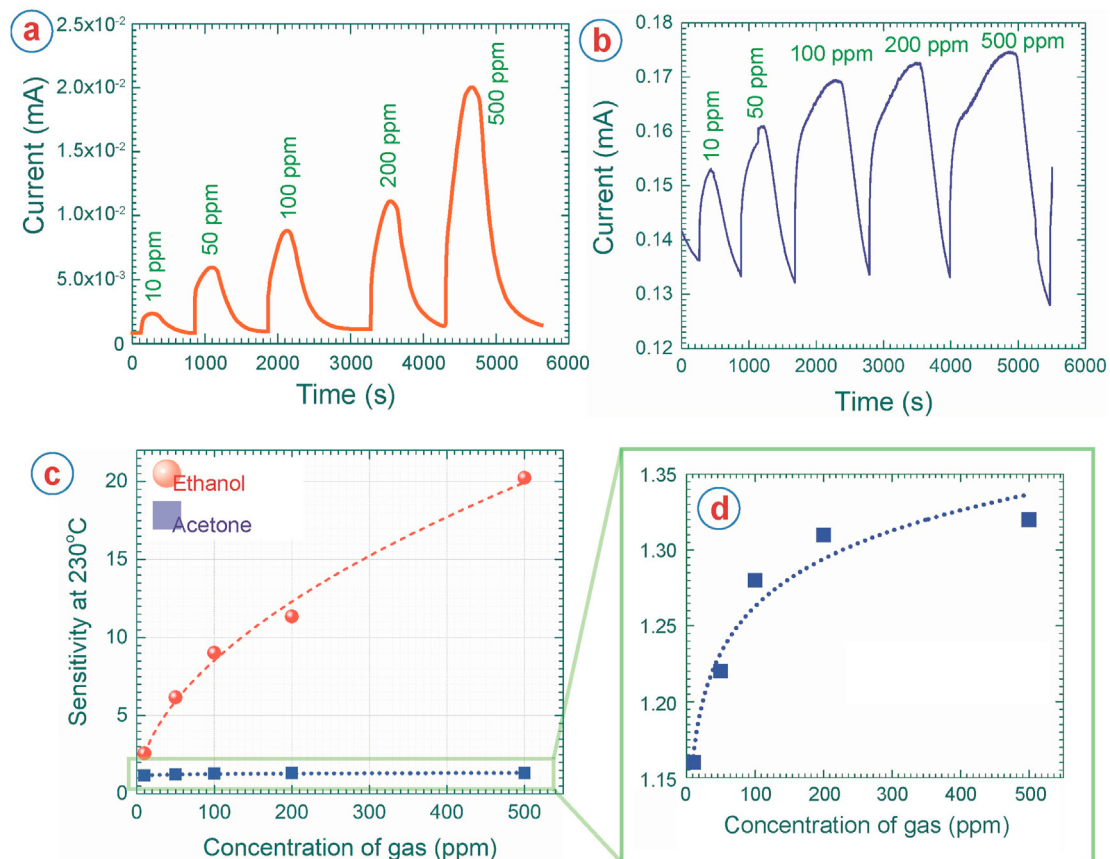


Fig. 5. The response and recovery of the ZnO nano-cactus sensors upon exposure to 10–500 ppm (a) ethanol and (b) acetone at 230 °C. (c) Sensitivity of the ZnO nano-cactus gas sensors for sensing of ethanol and acetone with increasing concentration of the gases at 230 °C. (d) Magnified view of the sensitivity of acetone for better clarification.

of 230 °C. The gas sensing response of the ZnO nano-cactus for ethanol is presented in Fig. 5a. A significant increase in the current was recorded during exposure to the gas. Such increase in the current was due to the chemical and electronic interaction between the gas and the ZnO nanostructures, which has been reported several times by other researchers [18,55–59]. Briefly, upon exposure to atmosphere, oxygen molecules present in the air are adsorbed on the surface of ZnO to form oxygen ions ( $O_2^-$ ,  $O^-$  and  $O^{2-}$ ) by capturing free electrons from the conduction band of ZnO. The lack of free electrons results in electron depletion regions at the surface, which consequently results in higher electrical resistance of the ZnO. Upon exposure to the target gas, the target gas gets adsorbed on the ZnO surface and reacts with the already adsorbed oxygen ions. The reaction between the adsorbed gas and oxygen ions produces excess free electrons at the surface, which results in lower resistance or higher electrical current [18]. The increase in the response increases proportionately with the gas concentration, as higher amount of target gas produces higher number of free electrons on the ZnO surface. Such response was also observed for the ZnO nano-cactus, as the response current increased with the increasing concentration of the target gas (Fig. 5a and b).

The sensitivity of the ZnO nano-cactus for both ethanol and acetone is shown in Fig. 5c and d. As expected, higher sensitivity was achieved with increasing the concentration of the gases. However, a significant difference in the sensitivity for ethanol and acetone was observed. The ZnO nano-cactus exhibited significantly higher sensitivity to ethanol than that for acetone. For ethanol, the sensitivity increased from 2.59 for 10 ppm to 20.23 for 500 ppm, whereas the sensitivity for acetone limits from 1.16 to 1.32 in the same concentration range. Hence, it is evident that the ZnO nano-cactus structures have a high selectivity to ethanol over acetone. This is promising as it can enable detection of ethanol gas from a gas mixture. However, the absolute value of the sensitivity obtained here is relatively lower than current state-of-the-art ZnO gas sensors. Such low gas sensitivity was due to use of lower operating temperature [60,61]. We used an operating temperature of 230 °C, whereas majority of the previous publications reported ethanol gas sensing performance at a temperature 250 °C or higher [62–66]. When we compare the sensitivity of ZnO gas sensors for ethanol around similar temperature we used here, we found that our ZnO nano-cactus exhibited relatively higher or comparable sensitivity to many of the previously reported ZnO gas sensors [60,61,63,65]. Furthermore, sensing at relatively low temperature implies lower power consumption for our system. It should be mentioned here that majority of the previous studies regarding gas sensing used 1 L of chamber for gas sensing characterization, whereas we used a cylindrical chamber of 3 L volume. This might result in slower response, but provides more practical approach for gas sensing. In addition to that, exhibiting high sensitivity in a large test chamber shows excellent functionality of ZnO nano-cactus as gas sensor element.

Such gas sensing performance of ZnO nano-cactus can be attributed to the “nano-on-micro” approach for the growth of ZnO nanostructures. Electrospun fibers are known to have a high specific surface area [25,26,67]. Using such electrospun fibers as the substrate for ZnO nanostructures growth, along with formation of long needle-like features of the ZnO nanocactus, increases the overall surface-to-volume ratio of the ZnO nanostructures. Increase in overall surface-to-volume ratio accommodates more gas molecules to interact with the sensor surface, which led to such excellent performance of the ZnO nano cactus for gas sensing at low temperature. Furthermore, “nano-on-micro” approach simplifies the sensor device fabrication. Majority of gas sensors reported in previous publications needed several post-synthesis steps to integrate the nanostructures with a sensing device, which included isolating of the nanostructures, preparing slurry and depositing it over a ceramic plate/cylinder with heater followed by annealing [23,24,68,69]. In comparison, synthesis of the nanostructure and sensor fabrication are combined in the “nano-on-micro” approach by fabricating the electrospun fibers on metallic track followed by growth of ZnO nanostructures on the fibers as shown in Fig. 1d. Therefore, no secondary steps are

needed for integration of the sensing material into a sensor system. Our further effort includes growth of ZnO nanowires around a single suspended nanofiber by using near-field electrospinning for the fiber deposition. Near-field electrospinning can enable precise deposition of a nanofiber across an electrode system [70]. Such system can potentially enable self-heating of the ZnO nanowires around the electrospun fiber, as joule heating of a suspended nanofiber can result in a temperature of up to 550 °C [71]. Hence, such system can increase the gas sensitivity significantly. Our future work is on achieving such system towards development of a self-heating high performance gas sensor.

#### 4. Conclusion

We successfully demonstrated a “nano-on-micro” approach for hierarchical cactus like growth of ZnO nanostructures around electrospun PAN/AuNP fibers using VLS method. The nano-cactus like features were obtained by controlling the reaction parameters in VLS method. Analytical characterization confirmed that wurtzite ZnO nanostructures were synthesized radially on the electrospun fibers. The “nano-on-micro” approach for ZnO nano-cactus growth resulted in excellent gas sensing properties at 230 °C. The nanostructures exhibited excellent sensitivity and selectivity towards ethanol gas sensing. Furthermore, the “nano-on-micro” approach proved to be a simple yet effective method for sensor integration, by enabling one-step nanostructure growth between electrodes and eliminating any need for post-synthesis processes.

#### Credit authorship contribution statement

Monsur Islam: Conceptualization of this study, Methodology, Data curation, Formal analysis, Writing – Original draft preparation, Writing - Revision of the manuscript. Alok K. Srivastava: Conceptualization of this study, Methodology, Data curation, Formal analysis, Writing - Revision of the manuscript. Basavanakote M. Basavaraja: Methodology, Data curation. Ashutosh Sharma: Supervision of the project.

#### Data availability

The raw/processed data required to reproduce these findings cannot be shared at this time due to legal or ethical reasons.

#### Declaration of competing interest

The authors declare that they have no known competing financial interests or personal relationships that could have appeared to influence the work reported in this paper.

#### References

- [1] E. Comini, G. Sberveglieri, Metal oxide nanowires as chemical sensors, *Mater. Today* 13 (7–8) (2010) 36–44.
- [2] A. Dey, Semiconductor metal oxide gas sensors: a review, *Mater. Sci. Eng., B* 229 (2018) 206–217.
- [3] P.R. Solanki, A. Kaushik, V.V. Agrawal, B.D. Malhotra, Nanostructured metal oxide-based biosensors, *NPG Asia Mater.* 3 (1) (2011) 17–24.
- [4] S. Das, V. Jayaraman, *Sno2*, A comprehensive review on structures and gas sensors, *Prog. Mater. Sci.* 66 (2014) 112–255.
- [5] L. Xiong, Y. Guo, J. Wen, H. Liu, G. Yang, P. Qin, G. Fang, Review on the application of *sno2* in perovskite solar cells, *Adv. Funct. Mater.* 28 (35) (2018) 1802757.
- [6] S. Rackauskas, N. Barbero, C. Barolo, G. Viscardi, ZnO nanowire application in chemoresistive sensing: a review, *Nanomaterials* 7 (11) (2017) 381.
- [7] P. Uikey, K. Vishwakarma, Review of zinc oxide (zno) nanoparticles applications and properties, *Int. J. Emerg. Technol. Comput. Sci. Electron.* 21 (2) (2016) 239–281.
- [8] K. Qi, B. Cheng, J. Yu, W. Ho, A review on *tio2*-based z-scheme photocatalysts, *Chin. J. Catal.* 38 (12) (2017) 1936–1955.
- [9] S.G. Ullattil, S.B. Narendranath, S.C. Pillai, P. Periyat, Black *tio2* nanomaterials: a review of recent advances, *Chem. Eng. J.* 343 (2018) 708–736.
- [10] S. Elouali, L.G. Bloor, R. Binions, I.P. Parkin, C.J. Carmalt, J.A. Darr, Gas sensing with nano-indium oxides (*in2o3*) prepared via continuous hydrothermal flow synthesis, *Langmuir* 28 (3) (2012) 1879–1885.

- [11] T. Waitz, T. Wagner, T. Sauerwald, C.-D. Kohl, M. Tiemann, Ordered mesoporous in2o3: synthesis by structure replication and application as a methane gas sensor, *Adv. Funct. Mater.* 19 (4) (2009) 653–661.
- [12] N. Yamazoe, New approaches for improving semiconductor gas sensors, *Sensor. Actuator. B Chem.* 5 (1–4) (1991) 7–19.
- [13] Y.-F. Sun, S.-B. Liu, F.-L. Meng, J.-Y. Liu, Z. Jin, L.-T. Kong, J.-H. Liu, Metal oxide nanostructures and their gas sensing properties: a review, *Sensors* 12 (3) (2012) 2610–2631.
- [14] A. Kolmakov, M. Moskovits, Chemical sensing and catalysis by one-dimensional metal-oxide nanostructures, *Annu. Rev. Mater. Res.* 34 (2004) 151–180.
- [15] T. Guo, M.-S. Yao, Y.-H. Lin, C.-W. Nan, A comprehensive review on synthesis methods for transition-metal oxide nanostructures, *CrystEngComm* 17 (19) (2015) 3551–3585.
- [16] Ü. Özgür, Y.I. Alivov, C. Liu, A. Teke, M. Reshchikov, S. Doğan, V. Avrutin, S.-J. Cho, H. Morkoç, A comprehensive review of zno materials and devices, *J. Appl. Phys.* 98 (4) (2005) 11.
- [17] U. Ozgur, D. Hofstetter, H. Morkoc, Zno devices and applications: a review of current status and future prospects, *Proc. IEEE* 98 (7) (2010) 1255–1268.
- [18] L. Zhu, W. Zeng, Room-temperature gas sensing of zno-based gas sensor: a review, *Sensor Actuator Phys.* 267 (2017) 242–261.
- [19] H. Wu, W. Pan, Preparation of zinc oxide nanofibers by electrospinning, *J. Am. Ceram. Soc.* 89 (2) (2006) 699–701.
- [20] J. Gonzalez-Chavarri, L. Parellada-Monreal, I. Castro-Hurtado, E. Castaño, G.G. Mandayo, Zno nanoneedles grown on chip for selective no2 detection indoors, *Sensor. Actuator. B Chem.* 255 (2018) 1244–1253.
- [21] X. Pan, X. Zhao, Ultra-high sensitivity zinc oxide nanocombs for on-chip room temperature carbon monoxide sensing, *Sensors* 15 (4) (2015) 8919–8930.
- [22] X.-B. Jin, Y.-X. Li, Y. Su, Z. Guo, C.-P. Gu, J.-R. Huang, F.-L. Meng, X.-J. Huang, M.-Q. Li, J.-H. Liu, Porous and single-crystalline zno nanobelts: fabrication with annealing precursor nanobelts, and gas-sensing and optoelectronic performance, *Nanotechnology* 27 (35) (2016) 355702.
- [23] H. Tian, H. Fan, J. Ma, Z. Liu, L. Ma, S. Lei, J. Fang, C. Long, Pt-decorated zinc oxide nanorod arrays with graphitic carbon nitride nanosheets for highly efficient dual-functional gas sensing, *J. Hazard Mater.* 341 (2018) 102–111.
- [24] L. Zhu, Y. Li, W. Zeng, Hydrothermal synthesis of hierarchical flower-like zno nanostructure and its enhanced ethanol gas-sensing properties, *Appl. Surf. Sci.* 427 (2018) 281–287.
- [25] Z.-M. Huang, Y.-Z. Zhang, M. Kotaki, S. Ramakrishna, A review on polymer nanofibers by electrospinning and their applications in nanocomposites, *Compos. Sci. Technol.* 63 (15) (2003) 2223–2253.
- [26] B. Ding, M. Wang, X. Wang, J. Yu, G. Sun, Electrospun nanomaterials for ultrasensitive sensors, *Mater. Today* 13 (11) (2010) 16–27.
- [27] T.J. Athauda, U. Butt, R.R. Ozer, One-dimensional hierarchical composite materials based on zno nanowires and electrospun blend nanofibers, *RSC Adv.* 3 (44) (2013) 21431–21438.
- [28] Ž. Petrović, M. Ristić, M. Marcius, M. Ivanda, V. Đurina, S. Musić, Hydrothermal processing of electrospun fibers in the synthesis of 1d zno nanoparticles, *Mater. Lett.* 176 (2016) 278–281.
- [29] B. Sun, X. Li, R. Zhao, H. Ji, J. Qiu, N. Zhang, D. He, C. Wang, Electrospun poly(vinylidene fluoride)-zinc oxide hierarchical composite fiber membrane as piezoelectric acoustoelectric nanogenerator, *J. Mater. Sci.* 54 (3) (2019) 2754–2762.
- [30] E. Matei, C. Busuioc, A. Evangelidis, I. Zgura, M. Enculescu, M. Beregoi, I. Enculescu, Hierarchical functionalization of electrospun fibers by electrodeposition of zinc oxide nanostructures, *Appl. Surf. Sci.* 458 (2018) 555–563.
- [31] F. Kayaci, S. Vempati, C. Ozgit-Akgun, N. Biyikli, T. Uyar, Enhanced photocatalytic activity of homoassembled zno nanostructures on electrospun polymeric nanofibers: a combination of atomic layer deposition and hydrothermal growth, *Appl. Catal. B Environ.* 156 (2014) 173–183.
- [32] J. Van Heerden, R. Swanepoel, Xrd analysis of zno thin films prepared by spray pyrolysis, *Thin Solid Films* 299 (1–2) (1997) 72–77.
- [33] J. Li, X. Chen, H. Li, M. He, Z. Qiao, Fabrication of zinc oxide nanorods, *J. Cryst. Growth* 233 (1–2) (2001) 5–7.
- [34] A.S. Lanje, S.J. Sharma, R.B. Ponde, Synthesis of silver nanoparticles: a safer alternative to conventional antimicrobial and antibacterial agents, *J. Chem. Pharmaceut. Res.* 2 (3) (2010) 478–483.
- [35] T.K. Sarma, D. Chowdhury, A. Paul, A. Chattopadhyay, Synthesis of an nanoparticle–conductive polyaniline composite using h<sub>2</sub>o<sub>2</sub> as oxidising as well as reducing agent, *Chem. Commun.* (10) (2002) 1048–1049.
- [36] S. Godipurge, S. Yallappa, N.J. Biradar, J. Biradar, B. Dhananjaya, G. Hegde, K. Jagadish, G. Hegde, A facile and green strategy for the synthesis of au, ag and au–ag alloy nanoparticles using aerial parts of r. hypocrateriformis extract and their biological evaluation, *Enzym. Microb. Technol.* 95 (2016) 174–184.
- [37] G. Yang, Z. Huang, X. Wang, B. Wang, Fabrication and anti-oxidation ability of sio<sub>2</sub> coated carbon fibers using sol-gel method, *Materials* 11 (3) (2018) 350.
- [38] M. Islam, P.G. Weidler, S. Heissler, D. Mager, J.G. Korvink, Facile template-free synthesis of multifunctional 3d cellular carbon from edible rice paper, *RSC Adv.* 10 (28) (2020) 16616–16628, <https://doi.org/10.1039/d0ra01447h>.
- [39] M. Islam, A.D. Lantada, M.R. Gañez, D. Mager, J.G. Korvink, Microarchitected carbon structures as innovative tissue engineering scaffolds, *Adv. Eng. Mater.* (2020) 2000083doi, <https://doi.org/10.1002/adem.202000083>.
- [40] I. Karacan, G. Erdoğdu, A study on structural characterization of thermal stabilization stage of polyacrylonitrile fibers prior to carbonization, *Fibers Polym.* 13 (3) (2012) 329–338, <https://doi.org/10.1007/s12221-012-0329-z>.
- [41] R. Zhang, P.-G. Yin, N. Wang, L. Guo, Photoluminescence and Raman scattering of zno nanorods, *Solid State Sci.* 11 (4) (2009) 865–869.
- [42] M. Šćepanović, M. Grujić-Brojčin, K. Vojisavljević, S. Bernik, T. Srečković, Raman study of structural disorder in zno nanopowders, *J. Raman Spectrosc.* 41 (9) (2010) 914–921.
- [43] R. Cuscó, E. Alarcón-Lladó, J. Ibanez, L. Artús, J. Jiménez, B. Wang, M.J. Callahan, Temperature dependence of Raman scattering in zno, *Phys. Rev. B* 75 (16) (2007) 165202.
- [44] J. Zi, H. Büscher, C. Falter, W. Ludwig, K. Zhang, X. Xie, Raman shifts in si nanocrystals, *Appl. Phys. Lett.* 69 (2) (1996) 200–202.
- [45] T. Zhai, S. Xie, Y. Zhao, X. Sun, X. Lu, M. Yu, M. Xu, F. Xiao, Y. Tong, Controllable synthesis of hierarchical zno nanodisks for highly photocatalytic activity, *CrystEngComm* 14 (5) (2012) 1850–1855.
- [46] R.S. Ganesh, E. Durgadevi, M. Navaneethan, V. Patil, S. Ponnusamy, C. Muthamizhchelvan, S. Kawasaki, P. Patil, Y. Hayakawa, Controlled synthesis of ni-doped zno hexagonal microdiscs and their gas sensing properties at low temperature, *Chem. Phys. Lett.* 689 (2017) 92–99.
- [47] S.-M. Li, L.-X. Zhang, M.-Y. Zhu, G.-J. Ji, L.-X. Zhao, J. Yin, L.-J. Bie, Acetone sensing of zno nanosheets synthesized using room-temperature precipitation, *Sensor. Actuator. B Chem.* 249 (2017) 611–623.
- [48] A.O. Dikovska, D. Pallotti, S. Lettieri, G. Atanasova, G. Avdeev, P. Maddalena, S. Amoroso, N. Nedyalkov, Growth mechanism of zno nanostructures produced by ultraviolet and visible laser ablation, *Appl. Surf. Sci.* 423 (2017) 977–982.
- [49] K. Guo, Property of zinc oxide (zno) nanostructures potential for biomedical system and its common growth mechanism, *J. Appl. Biotechnol. Bioeng.* 2 (5) (2017) 197–202.
- [50] C. Li, G. Fang, Q. Fu, F. Su, G. Li, X. Wu, X. Zhao, Effect of substrate temperature on the growth and photoluminescence properties of vertically aligned zno nanostructures, *J. Cryst. Growth* 292 (1) (2006) 19–25.
- [51] M.R. Khanlary, A. Reyhani, et al., Growth temperature dependence of vls-grown ultra-long zns nanowires prepared by cvd method, *J. Theor. Appl. Phys.* 12 (2) (2018) 121–126.
- [52] F.F. Comjani, U. Willer, S. Kontermann, W. Schade, Synthesis of zno nanowalls and nanocombs by vapor–liquid–solid method, *Phys. Status Solidi* 210 (10) (2013) 2219–2223.
- [53] F.-H. Chu, C.-W. Huang, C.-L. Hsin, C.-W. Wang, S.-Y. Yu, P.-H. Yeh, W.-W. Wu, Well-aligned zno nanowires with excellent field emission and photocatalytic properties, *Nanoscale* 4 (5) (2012) 1471–1475.
- [54] Z.R. Dai, Z.W. Pan, Z. Wang, Novel nanostructures of functional oxides synthesized by thermal evaporation, *Adv. Funct. Mater.* 13 (1) (2003) 9–24.
- [55] K. Korir, A. Cattellani, G. Cicero, Ethanol gas sensing mechanism in zno nanowires: an ab initio study, *J. Phys. Chem. C* 118 (42) (2014) 24533–24537.
- [56] N. Hongsith, E. Wongrat, T. Kercharoen, S. Chooon, Sensor response formula for sensor based on zno nanostructures, *Sensor. Actuator. B Chem.* 144 (1) (2010) 67–72.
- [57] W. Guo, T. Liu, H. Zhang, R. Sun, Y. Chen, W. Zeng, Z. Wang, Gas-sensing performance enhancement in zno nanostructures by hierarchical morphology, *Sensor. Actuator. B Chem.* 166 (2012) 492–499.
- [58] H. Bian, S. Ma, A. Sun, X. Xu, G. Yang, S. Yan, J. Gao, Z. Zhang, H. Zhu, Improvement of acetone gas sensing performance of zno nanoparticles, *J. Alloys Compd.* 658 (2016) 629–635.
- [59] M.S. Lemraski, E. Nadimi, Acetone gas sensing mechanism on zinc oxide surfaces: a first principles calculation, *Surf. Sci.* 657 (2017) 96–103.
- [60] Q. Wan, Q. Li, Y. Chen, T.-H. Wang, X. He, J. Li, C. Lin, Fabrication and ethanol sensing characteristics of zno nanowire gas sensors, *Appl. Phys. Lett.* 84 (18) (2004) 3654–3656.
- [61] L. Wang, Y. Kang, X. Liu, S. Zhang, W. Huang, S. Wang, Zno nanorod gas sensor for ethanol detection, *Sensor. Actuator. B Chem.* 162 (1) (2012) 237–243.
- [62] Q. Qi, T. Zhang, L. Liu, X. Zheng, Q. Yu, Y. Zeng, H. Yang, Selective acetone sensor based on dumbbell-like zno with rapid response and recovery, *Sensor. Actuator. B Chem.* 134 (1) (2008) 166–170.
- [63] J. Wang, J. Yang, N. Han, X. Zhou, S. Gong, J. Yang, P. Hu, Y. Chen, Highly sensitive and selective ethanol and acetone gas sensors based on modified zno nanomaterials, *Mater. Des.* 121 (2017) 69–76.
- [64] M. Ge, T. Xuan, G. Yin, J. Lu, D. He, Controllable synthesis of hierarchical assembled porous zno microspheres for acetone gas sensor, *Sensor. Actuator. B Chem.* 220 (2015) 356–361.
- [65] Y. Zhu, Y. Wang, G. Duan, H. Zhang, Y. Li, G. Liu, L. Xu, W. Cai, In situ growth of porous zno nanosheet-built network film as high-performance gas sensor, *Sensor. Actuator. B Chem.* 221 (2015) 350–356.
- [66] X. Xie, X. Wang, J. Tian, X. Song, N. Wei, H. Cui, Growth of porous zno single crystal hierarchical architectures with ultrahigh sensing performances to ethanol and acetone gases, *Ceram. Int.* 43 (1) (2017) 1121–1128.
- [67] I.S. Chronakis, Novel nanocomposites and nanoceramics based on polymer nanofibers using electrospinning process: a review, *J. Mater. Process. Technol.* 167 (2–3) (2005) 283–293.
- [68] R.L. Vander Wal, G. Hunter, J. Xu, M. Kulis, G. Berger, T. Tichich, Metal-oxide nanostructure and gas-sensing performance, *Sensor. Actuator. B Chem.* 138 (1) (2009) 113–119.

- [69] S. Choopun, A. Tubtimtae, T. Santhaveesuk, S. Nilphai, E. Wongrat, N. Hongsith, Zinc oxide nanostructures for applications as ethanol sensors and dye-sensitized solar cells, *Appl. Surf. Sci.* 256 (4) (2009) 998–1002.
- [70] X.-X. He, J. Zheng, G.-F. Yu, M.-H. You, M. Yu, X. Ning, Y.-Z. Long, Near-field electrospinning: progress and applications, *J. Phys. Chem. C* 121 (16) (2017) 8663–8678.
- [71] A. Cisuella-Serra, M. Gamero-Castaño, L. Ferrer-Argemi, J. Wardini, M. Madou, Controlled joule-heating of suspended glassy carbon wires for localized chemical vapor deposition, *Carbon* 156 (2020) 329–338.